CHEMISTRY WITHOUT SOLVENTS: PROPERTIES AND REACTIONS OF ORGANOMETALLIC COMPLEXES IN THE GAS PHASE

J. L. Beauchamp, Amy E. Stevens, and Reed R. Corderman

Arthur Amos Noyes Laboratory of Chemical Physics, California
Institute of Technology, Pasadena, California 91125, USA

Abstract - The application of ion cyclotron resonance spectroscopy to the study of organometallic reactions is described. Methodology is outlined for the determination of metal-hydrogen, metal-carbon and metal-ligand bond dissociation energies and representative results are given. These data are of fundamental importance in understanding the reactions of organic molecules at transition metal centers. Decarbonylation of aldehydes and dehydrogenation of alkanes are treated as examples of oxidative addition processes. Elimination of methane from hydrido methyl complexes exemplifies the study of reductive elimination reactions. Additional examples include studies of the acylation and alkylation of metal complexes, and the reactions of molecular hydrogen with several coordinatively unsaturated species.

INTRODUCTION

The growing field of organometallic chemistry is capturing the attention of an increasing number of researchers from both sides of this interface between organic and inorganic chemistry. In rendering the study of organic reactions a predictive science, organic chemists have benefitted enormously from the availability of quantitative data relating to bond strengths and acid-base properties of molecules. These data have been greatly expanded in recent years by studies utilizing ion cyclotron resonance spectroscopy (ICR) (Refs. 1-3) and high pressure mass spectrometry (Ref. 4). In contrast, there is a paucity of quantitative data relating to the energetics of metal-ligand interactions, including most importantly metal-hydrogen and metal-carbon bond dissociation energies (Refs. 5 & 6). The interpretation of organometallic reaction mechanisms and the design of new reagents and catalysts in other than an empirical fashion requires the availability of such data. In this brief account we summarize our efforts in applying the techniques of ion cyclotron resonance spectroscopy to the solution of this problem.

In addition to characterizing the nature and strengths of metal-ligand bonds, ICR studies have also revealed a rich chemistry associated with chemical transformations effected by the interaction of metal complexes with organic molecules. The variable oxidation states of transition metals are primarily responsible for their role as reagents and catalysts for organic reactions (Ref. 7). Not surprisingly, the most commonly observed processes other than ligand displacement reactions are oxidative addition and reductive elimination reactions. Examples of these processes are presented which illustrate the need for quantitive metal ligand bond strengths to interpret reactivity.

EXPERIMENTAL METHODS

In ion cyclotron resonance experiments, electric and magnetic fields are utilized to create an electromagnetic bottle in which charged particles can be stored for time periods up to several seconds (Ref. 8). Ions suffer collisions with neutrals at a rate of approximately one per second at 10^{-8} torr (Ref. 1). Hence, if reaction occurs at every encounter, reactants will be converted to products in 10 msec at 10^{-6} torr. In a typical experiment reactant ions are generated from a volatile precursor by a pulsed electron beam and stored for a suitable delay time or reaction period. Ion concentrations and masses are determined using the principle of ion cyclotron resonance in which absorption of energy from a radio frequency electric field occurs at the cyclotron frequency of the detected ion (Refs. 1 & 8). Positive or negative ions may be examined with equal facility. By varying the delay time, temporal profiles of ion concentrations are obtained. These are analyzed to yield information relating to the kinetics and thermochemistry of ion-molecule reactions (Refs. 1-3). These experiments are exemplified by the data shown in Fig. 1 for (η^5-cyclopentadienyl) nickel nitrosyl ionized by a 10 msec 70 eV electron beam pulse (Refs. 9 & 10). Reactions listed in Table 1 account for the variation of ion abundance with time in this system. Positive identification of reaction sequences is provided by double resonance experiments (Ref. 1). Rate constants are derived from the limiting slopes for the disappearance of
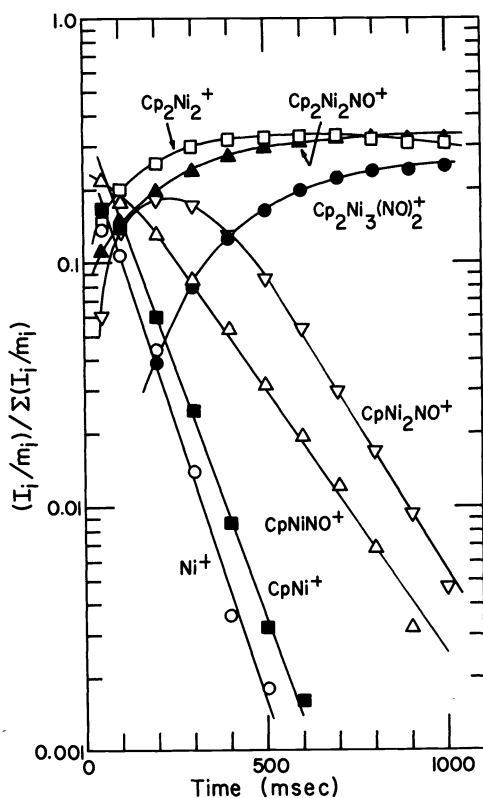
Fig. 1. Temporal variation of ion abundance in CpNiNO at 2.7×10^{-7} Torr following ionization by a 70 eV, 10 ms electron beam pulse. Minor ions are not shown.

TABLE 1. Ion-molecule reactions and rate constants for CpNiNO

Reaction	k^a
$CpNiNO^+ + CpNiNO \rightarrow Cp_2Ni_2NO^+ + NO$	5.8 ± 1.0
$CpNi^+ + CpNiNO \longrightarrow Cp_2Ni_2^+ + NO$	8.6 ± 1.0
$\qquad\qquad\qquad\longrightarrow CpNiNO^+ + CpNi$	1.7 ± 1.0
$Ni^+ + CpNiNO \rightarrow CpNi_2NO^+$	12.0 ± 2.0
$CpNi_2NO^+ + CpNiNO \rightarrow Cp_2Ni_3(NO)_2^+$	6.4 ± 1.0

^{a}Rate constants in units of 10^{-10} cm^{3}molecule^{-1}s^{-1}.

reactant ions (Ref. 8). A rate constant of 10^{-9} cm^{3}molecule^{-1}sec^{-1} typically corresponds to reaction on every collision. Several of the processes listed in Table 1 approach this limit. During the storage period ions may be irradiated with both lasers and conventional light sources, making it possible to study the spectroscopy and photochemistry of ions in the gas phase (Refs. 11 & 12). Details of the apparatus and experimental methods for these studies has been described in the literature (Refs. 1 & 8). Experiments described below were all performed at ambient temperature.

DETERMINATION OF METAL-HYDROGEN AND METAL-CARBON BOND DISSOCIATION ENERGIES

Techniques for the determination of base strengths toward the proton as a reference acid are well established (Ref. 13). The proton affinity of a base B, defined by the enthalpy change for reaction 1, serves to quantify gas phase base strengths. The base strengths of a

$$BH^+ \rightarrow B + H^+ \qquad \Delta H = PA(B) \tag{1}$$
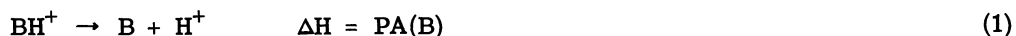
range of organometallic complexes (Refs. 14-20) are summarized in Table 2. In cases where protonation occurs on the metal center, these data directly yield metal-hydrogen bond dissociation energies, defined by the enthalpy change for homolytic bond cleavage, reaction 2. Equation 3 relates these quantities, where IP(B) is the adiabatic ionization potential of B. For the first six entries in Table 2 protonation on the metal is likely.

TABLE 2. Proton affinities and homolytic bond dissociation energies of organometallic complexes

Compound	Proton affinity[a] kcal/mole	IP eV	Homolytic BDE kcal/mole	Reference
$Fe(CO)_5$	204	7.98	74 ± 5	14
Cp_2Fe	213	6.8	56 ± 5	15
$(CO)_5MnCH_3$	188	8.3	67 ± 3	16
$(CH_3C_5H_4)Mn(CO)_3$	203	7.86	71 ± 3	17
$CpRh(CO)_2$	214	7.8	80 ± 5	18
$(CO)_5ReCH_3$	191	8.5	73 ± 3	19
CpNiNO	203	8.21	78 ± 3	10
Cp_2Ni	225	6.2	54 ± 3	20
U	238	6.19	67 ± 5	21
Ni	173	7.63	36 ± 10	22

[a]Relative to $PA(NH_3) = 207 \pm 2$ kcal mole^{-1} (Ref. 24).

$$BH^+ \rightarrow B^+ + H \qquad \Delta H = D(B^+ - H) \qquad (2)$$

$$D(B^+ - H) = PA(B) + IP(B) - IP(H) \qquad (3)$$

Metal-hydrogen bond dissociation energies fall in the range from 56 kcal/mole [ferrocene] to 80 kcal/mole [(η^5-cyclopentadienyl) rhodium dicarbonyl]. Estimates of metal hydrogen bond energies in neutral complexes generally fall in this same range (Refs. 5 & 6).

Also included in Table 2 are several metal hydrogen bond dissociation energies for diatomic metal hydride ions. These have been determined in our laboratory from measured thresholds for endothermic processes such as reaction 4 (Refs. 21 & 22).

$$U^+ + H_2 \rightarrow UH^+ + H \qquad (4)$$

Metal-carbon bond dissociation energies can be derived in a similar fashion by studies of alkylation reaction (Refs. 10 & 14). In the case of CpNiNO, a methyl cation affinity in the range 51 kcal/mole $< D(CpNiNO - CH_3^+) < 56$ kcal/mole has been determined (Ref. 10). This yields a rather low homolytic bond energy of 17 kcal/mole, which represents the metal carbon bond dissociation energy provided alkylation occurs on the metal center. The latter points out one of the difficulties of gas phase studies of ion-molecule reactions, namely, that structures must usually be inferred.

Allison and Ridge (Ref. 23) report limits on gas phase metal-carbon bond strengths of 68 kcal/mole $> D[M^+ - CH_3] > 56$ kcal/mole for M = Fe and Co.

### METAL-LIGAND BINDING ENERGIES

The first extensive ICR study of an organometallic complex, $Fe(CO)_5$, demonstrated that rapid displacement of CO by a variety of n- and π-donor bases occurs (Ref. 14). Although qualitative orderings could be inferred, rapid formation of polynuclear metal cluster complexes $Fe_n(CO)_m^+$ (n = 1-4; m = 0-12) precluded the determination of quantitative transition metal-ligand bond dissociation energies. Whereas polynuclear complexes are formed in the CpNiNO system, Fig. 1, it proved more attractive for the determination of metal-ligand binding energies (Refs. 9 & 10).

In cyclopentadienyl nickel nitrosyl alone, only the parent ion, $CpNiNO^+$, is observed at low electron energies (8.5-10.5 eV), and reacts with the precursor to yield $Cp_2Ni_2NO^+$ as indicated in Table 1. In the presence of excess base, B, fast ligand displacement reactions, such as generalized in Equation 5, are observed [e.g., $k = (1.4 \pm 0.3) \times 10^{-9}$ cm^{3}molecule^{-1}

$$CpNiNO^+ + B \rightarrow CpNiB^+ + NO \qquad (5)$$

s^{-1} for B = NH_3]. With a mixture of bases, attainment of equilibrium in transfer of $CpNi^+$

between B_1 and B_2 (equation 6) is observed to be rapid in comparison to any further reactions

$$CpNiB_1^+ + B_2 \rightleftharpoons \left[\begin{matrix} B_1 & B_2 \\ & Ni \end{matrix} \right]^+ \rightleftharpoons CpNiB_2^+ + B_1 \qquad (6)$$
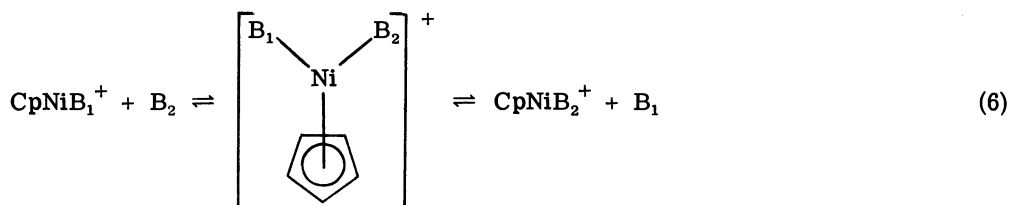
of the complexes with the neutrals present. The rapid exchange of monodentate n-donor ligands is promoted by the coordination vacancy of the 16-electron complex, $CpNiB^+$, which facilitates binding of a second pair donor to form the 18-electron intermediate indicated in equation 6. The displacement of a monodentate ligand by a bidentate or polydentate ligand (e.g., butadiene, benzene, and pyridine) results in the formation of an 18-(or more) electron complex which reacts very slowly, if at all, in further ligand exchange reactions.

The relative free energies of binding B_1 and B_2 can be determined from equilibria observed for process 6 with an accuracy of ± 0.2 kcal/mole for $\Delta G \leqslant 3$ kcal/mole. These data are converted to enthalpies by assuming ΔS is zero except for small corrections due to changes in symmetry numbers.

Representative data for binding energies of $CpNi^+$ to n-donor bases are shown in Fig. 2, where they are compared to proton binding energies for the same series of bases. Both
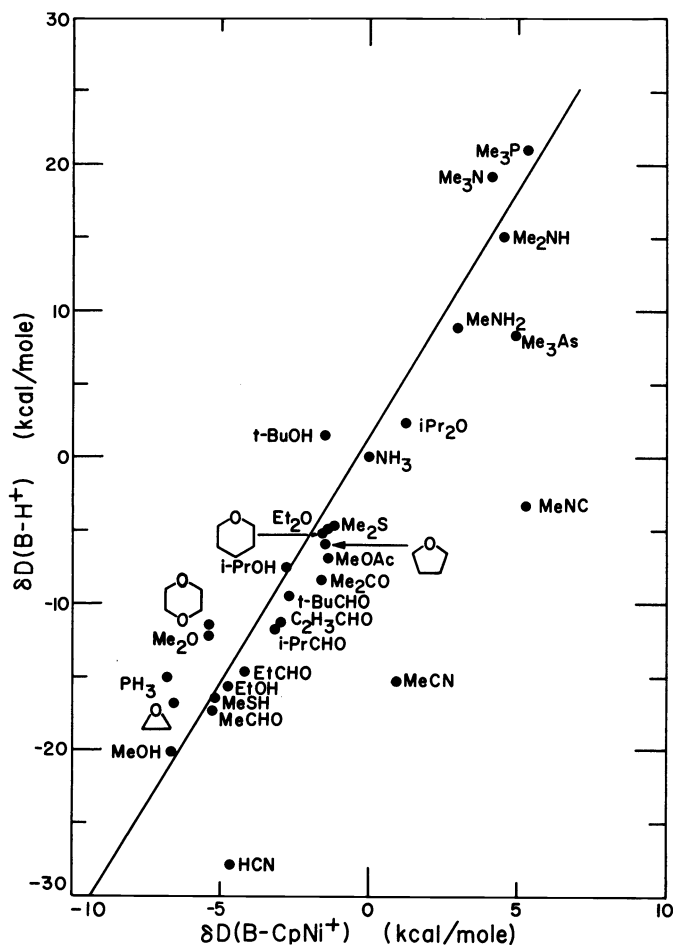

Fig. 2. Comparison of two scales of molecular basicity; binding energies of molecules to H^+, $\delta D(B-H^+)$, and to $CpNi^+$, $\delta D(B-CpNi^+)$. Binding energies are relative to NH_3 in each case.

sets of data are given relative to ammonia, for which absolute values $D[NH_3 - NiCp^+] = 52.3 \pm 2$ kcal/mole (Refs. 9 & 10) and $PA(NH_3) = 207 \pm 2$ kcal/mole (Ref. 24) have been determined.

Several trends in $D(B-CpNi^+)$ are apparent from the data in Fig. 2. $D(B-CpNi^+)$ generally increases with increasing substitution of alkyl groups for H on the basic site ($Me_3P > PH_3$, $Me_2O > MeOH > H_2O$, $Me_2S > MeSH > H_2S$). Interestingly, the

$D(B-CpNi^+)$ ordering of the alkyl amine series is irregular, with $Me_2NH > Me_3H > MeNH_2 > NH_3$, similar to the behavior the amines exhibit towards Li^+ (Ref. 25). $D(B-CpNi^+)$ increases with increasing methyl substitution on the carbon α to the basic site ($Me_3COH > Me_2CHOH > EtOH > MeOH$, $Et_2O > Me_2O$, $MeCN > HCN$). $D(B-CpNi^+)$ increases with increasing alkyl substitution on carbon remote to the basic site ($Me_2CCHO > Me_2CHCHO > MeCH_2CHO > CH_3CHO$). Finally, $D(B-CpNi^+)$ is greater for second-row n-donor ligands than for first-row species ($Me_3P > Me_3N$, $Me_2S > Me_2O$).

The metal-ligand bond dissociation energies are most striking in their comparison to proton affinities. Excluding the compounds NO, HCN, MeCN, MeNC, and Me_3As, a surprisingly good linear correlation (correlation coefficient 0.964) is observed (Fig. 2, equation 7).

$$\delta D(B-NiCp^+) = 0.296\ \delta D(B-H^+) - 0.453 \tag{7}$$

The correlation may be of predictive value, e.g., from $\delta D(H_2O-H^+) = -32.0$ kcal/mole, $\delta D(H_2O-NiCp^+) = -9.9$ kcal/mole is obtained.

The notable exceptions to the observed correlation of metal-ligand bond dissociation energies with proton affinities occurs for ligands which participate in π-bonding with metal centers. In all cases the deviation indicates a stronger interaction with the metal center relative to the proton.

Recent semiempirical molecular orbital calculations of the electronic structure of $M(CH)_n$ (n = 3-8) and $M(CO)_3$ fragments lead to a qualitative description of the bonding in $CpNi^+$ and $CpNiB^+$ species. For $CpNiB^+$, bonding occurs primarily through ligand-to-metal σ donation into the empty 4s orbital on the metal. For those ligands with filled π orbitals (NO, HCN, MeCN, MeNC, and Me_3As), delocalization of the ligand π electrons into the empty metal e_1 (d_{xz} and d_{yz}) orbitals may occur, stabilizing the charge on nickel and leading to a stronger metal-ligand bond (Ref. 26).

An obvious extension of the above study considers a system with two exchangeable sites. The complex $CpFe(CO)_2CH_3$ has proven ideal for such investigations (Ref. 27). Reactions of proton donors with this species lead to the formation of $CpFe(CO)_2^+$, which rapidly exchanges both CO ligands with n-donor bases. With two bases present there will be three possible complexes formed. The relative abundance of these complexes will be determined in part by interactions between the two ligands as indicated in Fig. 3. Steric effects may favor small ligands over ligands with bulky substituents. Electrostatic repulsion would render a complex with two highly polar ligands unfavorable. Synergistic effects may also be observed, with pure σ-donor ligands increasing the electron density available on the metal center for back bonding to π-acceptors. As an example of such studies, the two ligands acetaldehyde and dimethyl ether have nearly equal binding energies to $CpNi^+$ (Fig. 2). None of the special effects indicated in Fig. 3 should be important. Consequently in a mixture

Steric Effects

Electrostatic Interactions
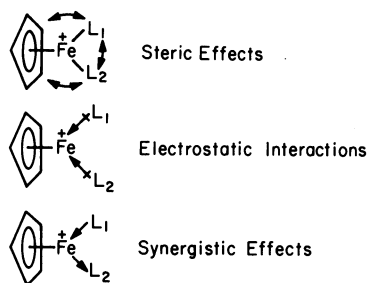
Synergistic Effects

Fig. 3. Possible modes of ligand interaction in $CpFeL_1L_2^+$ complexes.

containing CH_3CHO and CH_3OCH_3 in a 1:1 ratio the three complexes $CpFe(CH_3CHO)_2^+$, $CpFe(CH_3OCH_3)(CH_3CHO)^+$ and $CpFe(CH_3OCH_3)_2^+$ should be observed in a statistical ratio of 1:2:1. This is very close to the observed ratio at long times (Fig. 4). In general the data for ligand binding to $CpNi^+$ has been found to be transferable to other cationic systems with several binding sites, provided none of the interesting effects noted in Fig. 3 are operative.

ENERGETICS AND MECHANISMS OF ORGANOMETALLIC REACTIONS

Oxidative addition processes

During the course of investigating metal ligand bond dissociation energies, many interesting reactions of the abundant fragment ion $CpNi^+$ with organic molecules were observed (Ref. 10). Processes examined include sequential alkylation of the reactant ion (Ref. 28), decarbonylation of aldehydes (Ref. 29), and elimination reactions as illustrated below. Studies of the mechanism of these processes suggest in every case an initial step involving oxidative insertion of $CpNi^+$ into polar C—X bonds (X = H, Cl, Br, I, OH) (Ref. 10). Perhaps the most intriguing of the reactions observed for $CpNi^+$ is the decarbonylation of
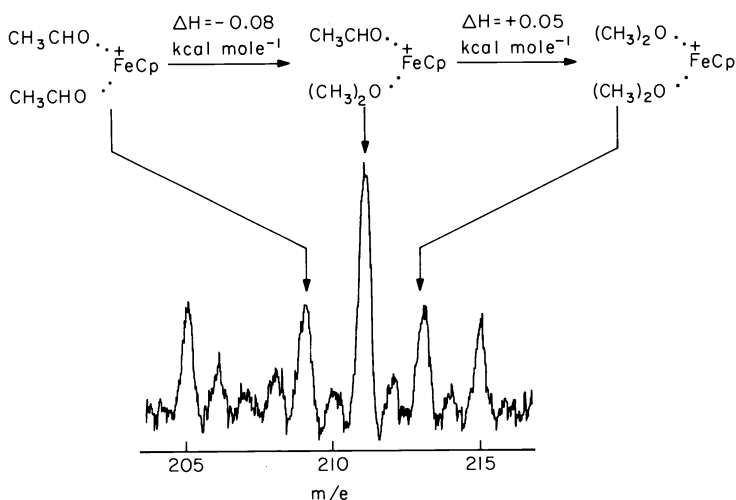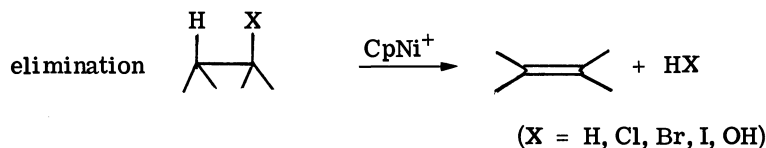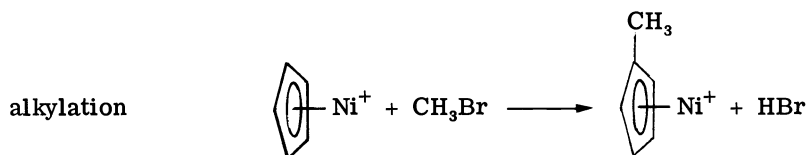
Fig. 4. Single resonance ICR mass spectrum showing complexes observed at equilibrium with a 1:1 mixture of CH_3CHO and CH_3OCH_3 as neutral ligands. These ligands displace CO from $CpFe(CO)_2^+$ formed as described in the text.

alkylation

decarbonylation $RCHO \xrightarrow{CpNi^+} RH + CO$

elimination

$(X = H, Cl, Br, I, OH)$

aldehydes (Ref. 29) to hydrocarbons and CO, generalized in Equation 8 and 9. Reaction 8

$$CpNi^+ + RCHO \begin{cases} CpNiCO^+ + RH & \text{(8)} \\ CpNiRH^+ + CO & \text{(9)} \end{cases}$$
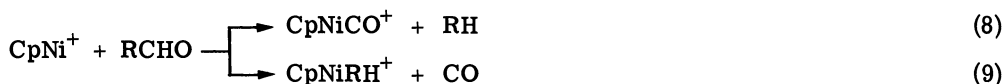
is observed for RCHO = MeCHO, EtCHO, i-PrCHO, and t-BuCHO. $CpNiRH^+$ is observed with RCHO = 3-methyl acrolein and benzaldehyde. Decarbonylation reactions are not observed for H_2CO, CF_3CHO, CH_3COCl, CH_3COBr, Me_2CO, and MeOAc.

These results lead to several conclusions concerning decarbonylation reactions effected by $CpNi^+$. The reaction mechanism is specific for aldehydes, as none of the molecules CH_3COX (X = Cl, Br, CH_3, OCH_3) are decarbonylated. This suggests that hydrogen on the acyl carbon is important, since product ions which result from facile X^- transfer to nickel are observed only for X = H, and not for X = Cl, Br, CH_3, OCH_3. A measure of acyl carbon-hydrogen bond strengths is given by the hydride affinity, $D(RCO^+-H^-)$, of these cations. Using available thermochemical data, it is apparent that when $D(RCO^+-H^-)$ becomes greater than ~ 250 kcal/mole, decarbonylation is not observed, presumably because hydride transfer to $CpNi^+$ does not occur. The weaker of the two bonds $CpNi(RH)^+-CO$ or $CpNi(CO)^+-RH$ will be preferentially broken in the final step of the

reaction.

An energy profile diagram and proposed intermediates for the decarbonylation of acetaldehyde is shown in Fig. 5 (Ref. 29). The initial interaction of $CpNi^+$ with CH_3CHO produces

CpNi⁺ + MeCHO

$E^* = 47$ kcal/mole

$\Delta H = -45$ kcal/mole

$CpNiCO^+ + CH_4$

I II III IV

$$CpNi\cdots O=C\underset{H}{\overset{CH_3}{<}} \quad CpNi\underset{H}{\overset{+}{<}}\overset{\overset{O}{\parallel}}{C}CH_3 \quad CpNi\underset{H}{\overset{+}{<}}\overset{CO}{CH_3} \quad CpNi\underset{CH_4}{\overset{+}{<}}\overset{CO}{}$$
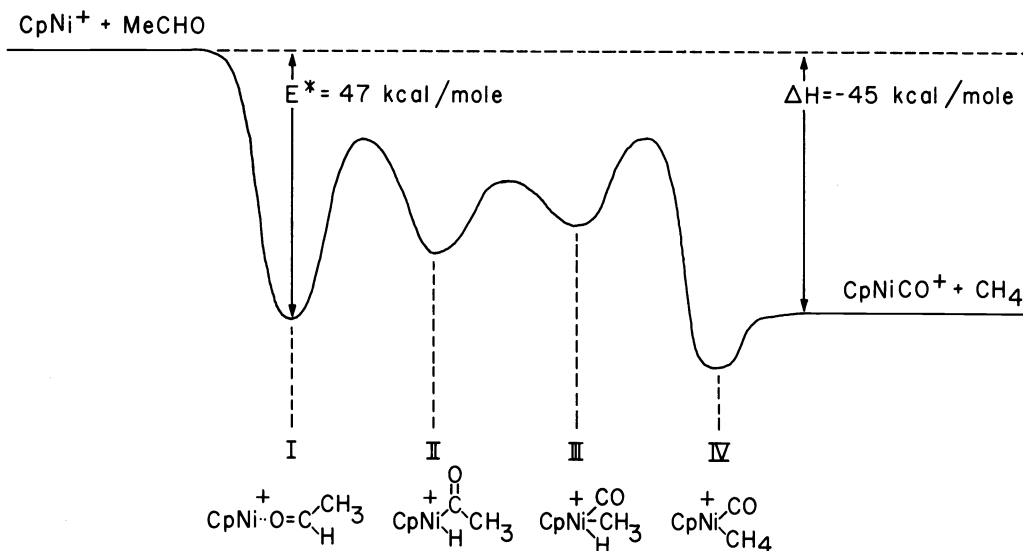
Fig. 5. Proposed energy profile diagram and reaction intermediates for the decarbonylation of acetaldehyde by $CpNi^+$.

the chemically activated species I with an internal energy of 47 kcal/mole. This is sufficient to allow for oxidative insertion of the metal into the C−H bond yielding II. While formation of CH_4 may result from a four center process starting with II, it is more likely that this is preceded by migration of CH_3 onto the metal, giving rise to intermediate III. The intermediate species IV results from the expected weak interaction of CH_4 with $CpNiCO^+$. The stabilities of the intermediates II and III and the height of the barriers connecting these species to I and IV remain unknown.

$CpNi^+$ will dehydrogenate species ranging from propane to diethylamine. The dehydrogenation of cyclopentane to both cyclopentene and cyclopentadiene (Equations 10 and 11) exemplifies these processes. The energy profile diagram presented in Fig. 6 summarizes
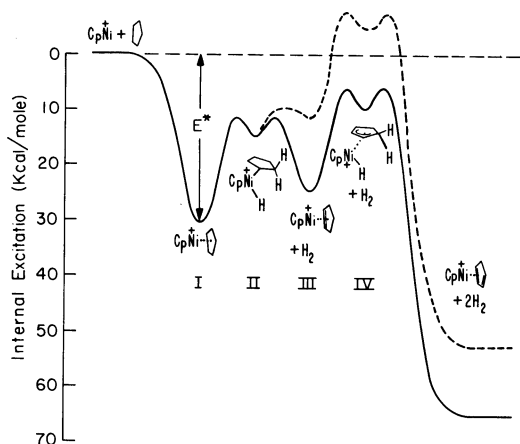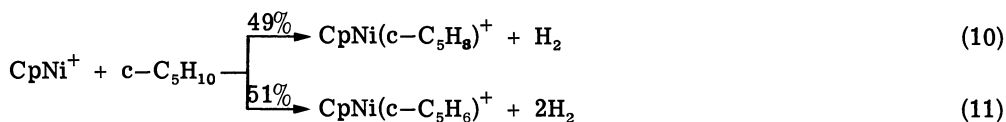
$$CpNi^+ + c-C_5H_{10} \longrightarrow \begin{cases} \xrightarrow{49\%} CpNi(c-C_5H_8)^+ + H_2 & (10) \\ \xrightarrow{51\%} CpNi(c-C_5H_6)^+ + 2H_2 & (11) \end{cases}$$


Fig. 6. Proposed energy profile diagram for the energetic changes associated with the dehydrogenation of cyclopentane by $CpNi^+$. The dashed curve results from the loss of H_2 in the v = 1 level from intermediate II.

energetic changes associated with the dehydrogenation of cyclopentane by $CpNi^+$. The initial interaction results in the formation of a weakly bound $CpNi(c-C_5H_{10})^+$ complex, I. The internal excitation of intermediate I is estimated to be approximately $E^* \approx 30$ kcal/mole. Intermediate II results from hydride transfer and subsequent oxidative insertion of nickel into the C—H bond. Hydrogen elimination involving hydrogen on the metal and cyclopentyl hydrogen endo to nickel produces $CpNi(c-C_5H_8)^+$, III. Formation of $CpNi(c-C_5H_8)^+$ produces a species with an internal excitation of approximately 23 kcal/mole [assuming $D(c-C_5H_8-CpNi^+) \approx 49 \pm 5$ kcal/mole as for isobutylene], and dehydrogenates further to $CpNi(c-C_5H_6)^+$, or protonated nickelocene. The dashed curve would result from the loss of H_2 in the $v = 1$ level (4395 cm^{-1} = 12.6 kcal/mole); in this case loss of a second H_2 molecule is not energetically possible. Loss of energy to translation (product repulsion) would give similar results. From the observed product distribution in 49% of the reactions the loss of the first H_2 molecule removes sufficient internal excitation to inhibit loss of a second.

Reductive elimination reactions

The reductive elimination of alkanes from organometallic complexes is an important class of reactions for which the mechanism remains controversial in many instances. This is due in part to the difficulties in characterizing reactive intermediates in solution. Treatment of transition metal alkyl complexes with acids in solution often leads to the evolution of alkanes. Pentacarbonylmethylmanganese is one compound which shows this reactivity; it decomposes rapidly in acidic media with methane evolution (Refs. 30 & 31). Studies of the protonation of $(CO)_5MnCH_3$ in the gas phase provide interesting insights into both the mechanism and energetics of methane formation in this system (Ref. 16).

Reaction of a variety of proton donors BH^+ with $(CO)_5MnCH_3$ yields two products, as indicated by Equations 12 and 13. At first glance the product of reaction 12 appears to involve

$$(CO)_5MnCH_3 + BH^+ \begin{cases} \longrightarrow (CO)_5Mn^+ + CH_4 + B & (12) \\ \longrightarrow (CO)_5Mn(CH_3)H^+ + B & (13) \end{cases}$$
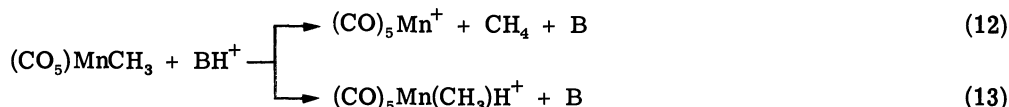
loss of CH_4 from the conjugate acid formed in reaction 13. The usual situation in proton transfer reactions, generalized in Equation 14, is for proton transfer from B_1 to B_2 to occur

$$B_1H^+ + B_2 \rightleftharpoons B_2H^+ + B_1 \tag{14}$$

when $PA(B_2) \geq PA(B_1)$. When the reaction is sufficiently exothermic, excess energy retained by B_2H^+ results in its decomposition. With this expected behavior, the results are interesting in that the conjugate acid $(CO)_5Mn(CH_3)H^+$ is observed only with bases whose proton affinity is substantially below those which yield the product $(CO)_5Mn^+$ as an abundant ion.

The important features of the observed reactions, as illustrated in Fig. 7, are as follows: Methane elimination takes place with proton donors for which $PA(B) \leq 203 \pm 3$ kcal/mole. Onset of reaction 13 establishes a proton affinity of $(CO)_5MnCH_3$ as 188 ± 3 kcal/mole. If the proton transfer reaction is sufficiently exothermic, internal excitation of the product of reaction 13 may be sufficient for dissociation to occur (Equation 15), in which CO is lost in

$$[(CO)_5Mn(CH_3)H^+]^* \rightarrow (CO)_4Mn(CH_3)H^+ + CO \tag{15}$$
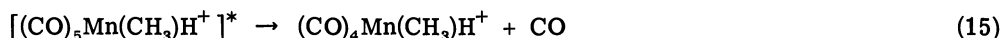
preference to CH_4. Decomposition according to reaction 15 is observed with donors less basic than HCN. This result indicates $D[(CO)_4Mn(CH_3)(H)^+ - CO] \sim 7 \pm 2$ kcal/mole.

These data are consistent with two available reactive sites on $(CO)_5MnCH_3$; reactions 1 and 2 are not competitive in the sense of having common or readily interconverted intermediates. We propose that protonation of the manganese-methyl bond leads to formation of methane with little or no activation barrier. Protonation at a second site, accessible with stronger proton donors, forms a kinetically stable protonated complex. Solution data on protonation of similar species lead us to believe the $(CO)_5Mn(CH_3)H^+$ ion is a hydridomethyl species with the proton on the metal center. The manganese-hydride bond dissociation energy of 67 ± 3 kcal/mole is comparable to those of other first row transition metal hydrides (Table 2). The elimination of methane from $[(CO)_5Mn(CH_3)H^+]$ is not competitive with loss of CO. The above data indicate an activation energy for reductive elimination in excess of 7 ± 2 kcal/mole. These results are summarized in Fig. 8, where the activation energy E_a for elimination of methane from $(CO)_5Mn(CH_3)H^+$ is unknown.

Reactions of Hydrogen with organometallic complexes

In studies of organometallic reactions involving first row transition metals we have searched for but not observed processes involving the reaction of molecular hydrogen at transition metal centers in mononuclear complexes. Such reactions occur readily with rhodium complexes, however. Protonation of $CpRh(CO)_2$ leads to formation of the ions $CpRh(CO)_nH^+$, $n = 0-2$, with loss of CO becoming more prominent as the proton affinity of the donor base
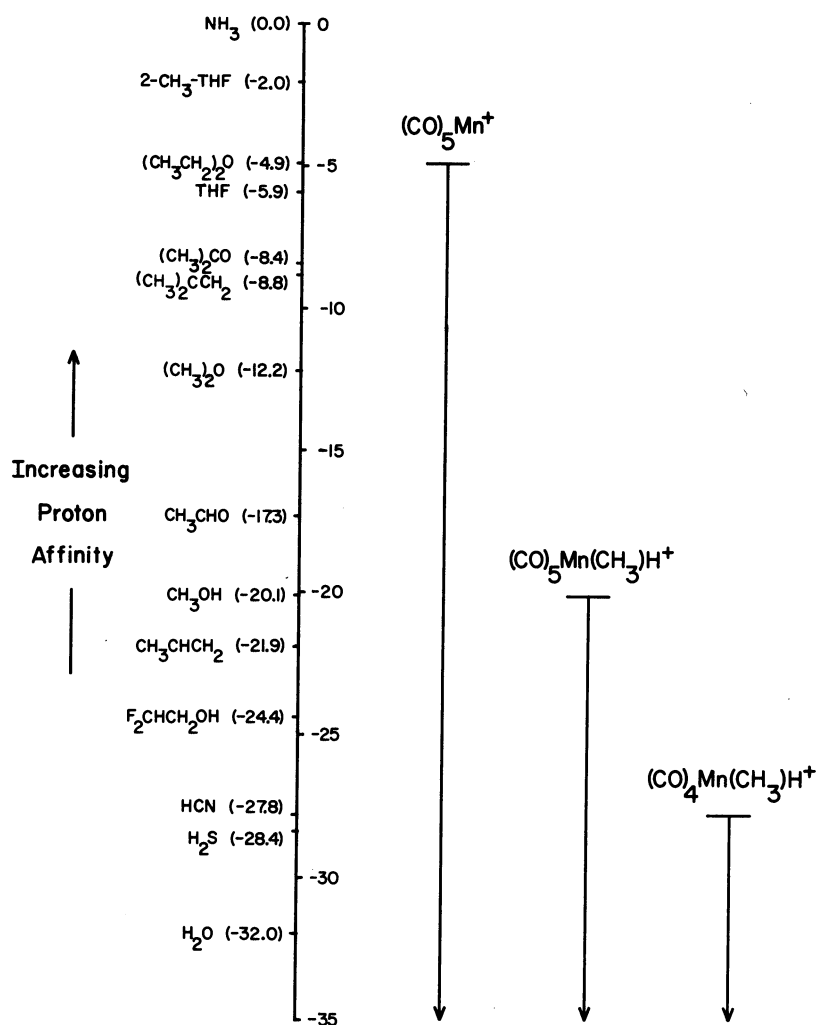
Fig. 7. Range of proton donors for which the products $(CO)_5Mn^+$ (reaction (12), $(CO)_5Mn(CH_3)H^+$ (reaction 13) and $(CO)_4Mn(CH_3)H^+$ (reaction 15) are observed. The proton affinity (kcal/mole) of each base examined, PA(B) -PA(NH$_3$), is given in parentheses (Ref. 13).
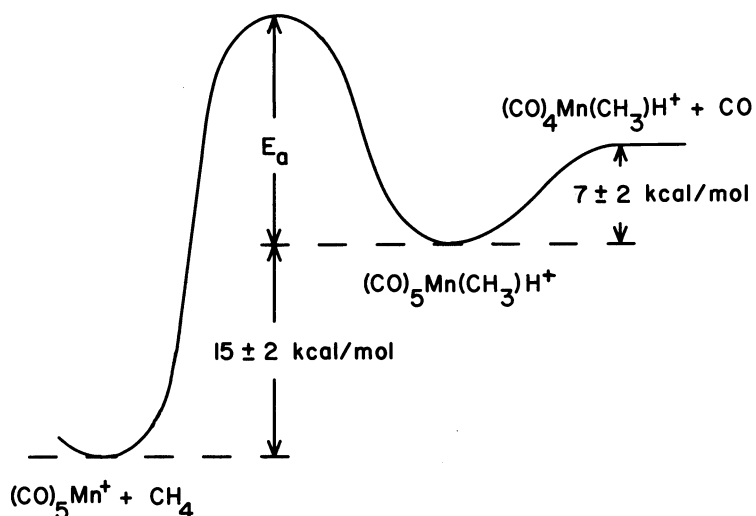

Fig. 8. Energetic relationships between species resulting from reductive elimination of CH_4 or loss of CO from protonated $(CO)_5MnCH_3$.

is decreased (Ref. 18). The species $CpRhH^+$ is particularly reactive in the dehydrogenation of alkanes. When formed with $B = D_2$, this species reacts with cyclopentane to yield mainly rhodocene (Equation 16); no deuterium is incorporated in the product. Dehydrogenation of
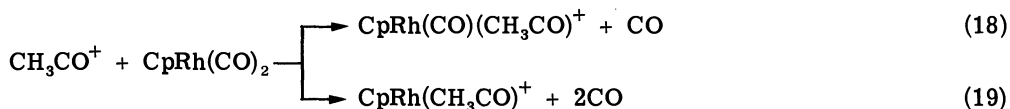
$$CpRhD^+ + c-C_5H_{10} \rightarrow Cp_2Rh^+ + HD + 2H_2 \tag{16}$$

propane yields what is presumably a π-allyl complex (Equation 17). When $CpRh(CO)H^+$ is

$$CpRhD^+ + C_3H_8 \rightarrow CpRh(C_3H_5)^+ + HD + 2H_2 \tag{17}$$
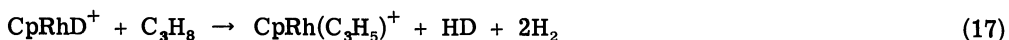
formed by reaction of $CpRh(CO)_2$ with CH_5^+, subsequent reaction with D_2 leads to incorporation of a single deuterium into the ionic product. Similarly the ionic product of reaction 17 incorporates four deuterium atoms when D_2 is present. The mechanism proposed for these reactions is as indicated below, with the first step involving addition of D_2 to the metal center.
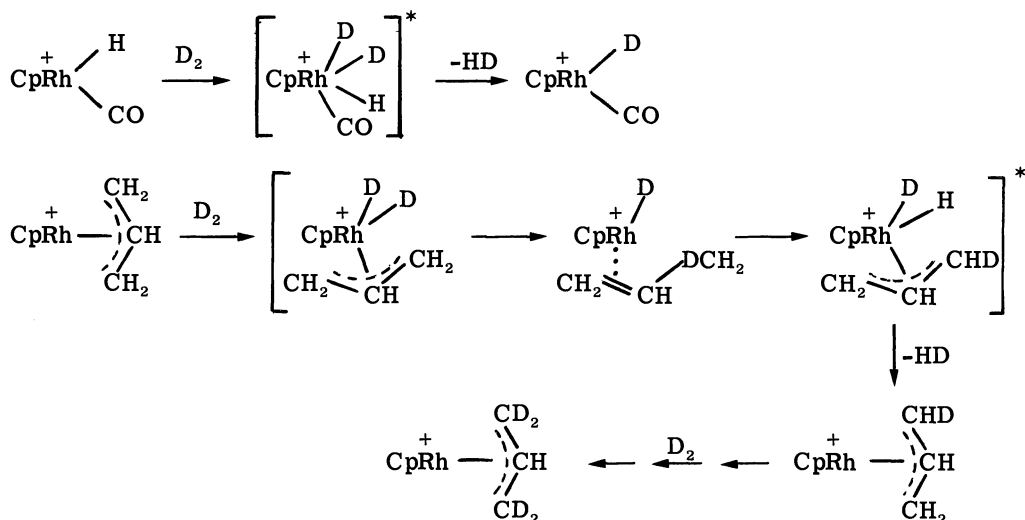
Acylation of $CpRh(CO)_2$ with CH_3CO^+ leads to the two products indicated in Equations 18 and 19. Using ^{18}O labelled CH_3CO^+, all of the label is retained in the ionic product of reaction

$$CH_3CO^+ + CpRh(CO)_2 \begin{cases} \rightarrow CpRh(CO)(CH_3CO)^+ + CO \tag{18} \\ \rightarrow CpRh(CH_3CO)^+ + 2CO \tag{19} \end{cases}$$

18 and exactly one half is present in the ionic product of reaction 19. CO can be displaced from the ionic product of reaction 19 with strong n-donor bases. Methylation of $CpRh(CO)_2$ with the dimethyl fluoronium ion (Ref. 32) leads to abundant formation of $CpRh(CO)CH_3^+$. This species reacts rapidly with D_2 as does the product of reaction 19 to yield the hydrido species $CpRh(CO)D^+$. This sequence of reactions is illustrated by the trapped ion data shown in Fig. 9. The reaction scheme proposed below accounts for the acylation and alkylation of $CpRh(CO)_2$. It is evident in the acylation process that methyl migration from carbon to metal precedes loss of the second CO.

The chemistry of $CpRh(CO)_2$ differs significantly from previous investigations of first row complexes in that hydrogen reversibly binds and dissociates on <u>coordinately unsaturated</u> rhodium complexes without an apparent activation energy. With <u>metal alkyl complexes</u> this leads to the reductive elimination of alkanes in preference to loss of CO. This contrasts the behavior discussed above for protonated $(CO)_5MnCH_3$. Since these differences in reactivity are intimately related to metal ligand bond dissociation energies, it is not surprising that the strongest metal hydrogen bond thus far examined is for the rhodium complex $CpRh(CO)_2$ listed in Table 2.

PROGNOSIS

New experimental techniques, including most prominently ion cyclotron resonance spectroscopy, have created a mini-renaissance in physical organic chemistry during the last decade. With the determination of properties such as proton affinities, carbonium ion stabilities, acidities, bond dissociation energies, and electron affinities, new insights into the reactivity of organic molecules in the absence of solvent have been attained. The
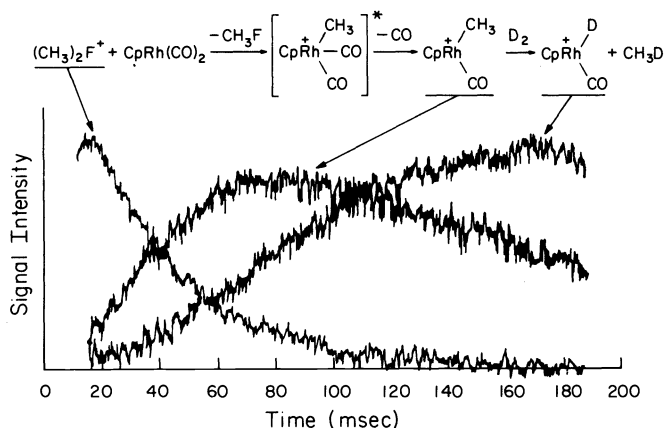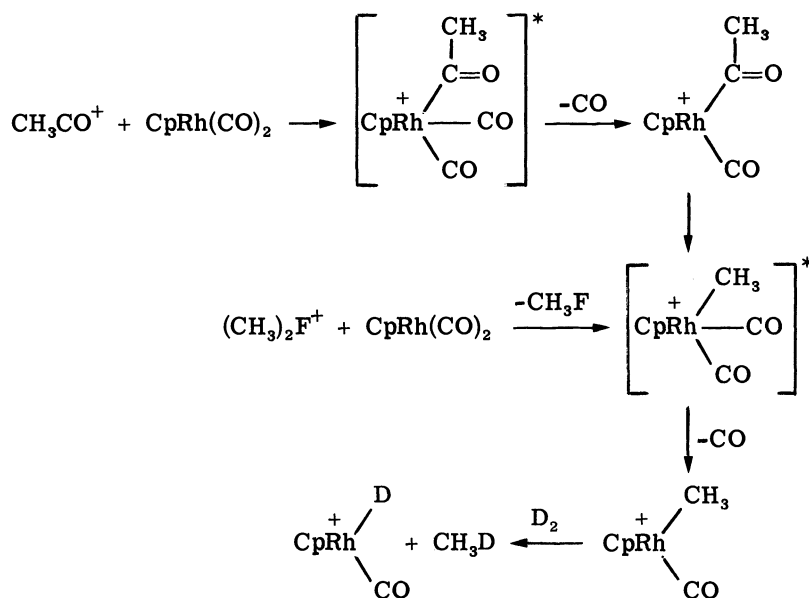
$$\text{(CH}_3)_2\text{F}^+ + \text{CpRh(CO)}_2 \xrightarrow{-\text{CH}_3\text{F}} \left[\begin{array}{c} \text{CH}_3 \\ \overset{+}{\text{CpRh}}\text{---CO} \\ | \\ \text{CO} \end{array} \right]^{*} \xrightarrow{-\text{CO}} \overset{+}{\text{CpRh}}\begin{array}{c} \text{CH}_3 \\ \diagup \\ \diagdown \\ \text{CO} \end{array} \xrightarrow{\text{D}_2} \overset{+}{\text{CpRh}}\begin{array}{c} \text{D} \\ \diagup \\ \diagdown \\ \text{CO} \end{array} + \text{CH}_3\text{D}$$

Fig. 9. Trapped ion data for a mixture of $CpRh(CO)_2$, CH_3F, and D_2, illustrating species involved in the alkylation of $CpRh(CO)_2$ and subsequent hydrogen reduction of $CpRh(CO)CH_3^+$.

$$\text{CH}_3\text{CO}^+ + \text{CpRh(CO)}_2 \longrightarrow \left[\begin{array}{c} \text{CH}_3 \\ | \\ \text{C=O} \\ \overset{+}{\text{CpRh}}\text{----CO} \\ \diagdown \\ \text{CO} \end{array} \right]^{*} \xrightarrow{-\text{CO}} \overset{+}{\text{CpRh}}\begin{array}{c} \text{CH}_3 \\ | \\ \text{C=O} \\ \diagup \\ \diagdown \\ \text{CO} \end{array}$$

$$\text{(CH}_3)_2\text{F}^+ + \text{CpRh(CO)}_2 \xrightarrow{-\text{CH}_3\text{F}} \left[\overset{+}{\text{CpRh}}\begin{array}{c} \text{CH}_3 \\ \diagup \\ \text{----CO} \\ \diagdown \\ \text{CO} \end{array} \right]^{*}$$

$$\downarrow -\text{CO}$$

$$\overset{+}{\text{CpRh}}\begin{array}{c} \text{D} \\ \diagup \\ \diagdown \\ \text{CO} \end{array} + \text{CH}_3\text{D} \xleftarrow{\text{D}_2} \overset{+}{\text{CpRh}}\begin{array}{c} \text{CH}_3 \\ \diagup \\ \diagdown \\ \text{CO} \end{array}$$

impact which these techniques will have on inorganic and organometallic chemistry will very likely be even greater. The selected examples presented above can only whet one's appetite for what is now possible.

REFERENCES

1. J. L. Beauchamp, in Annual Reviews of Physical Chemistry, H. Eyring (ed.), Vol. 22, 527-561, Annual Reviews, Palo Alto (1971).
2. J. L. Beauchamp, in Interactions Between Ions and Molecules, P. Ausloos (ed.), 413-444, Plenum, New York (1975).
3. T. A. Lehman and M. M. Bursey, Ion Cyclotron Resonance Spectrometry, John-Wiley, New York (1976).
4. P. Kebarle, in Annual Reviews of Physical Chemistry, H. Eyring (ed.), Vol. 28, 445-476, Annual Reviews, Palo Alto (1977).
5. J. A. Connor, Topics in Current Chemistry 71, 71-110 (1977).
6. H. A. Skinner, Advances in Organometallic Chemistry 2, 49-114 (1964).
7. R. F. Heck, Organotransition Metal Chemistry: A Mechanistic Approach, Academic Press, New York (1974).
8. T. B. McMahon and J. L. Beauchamp, Rev. Sci. Instr. 43, 509-512 (1972).
9. R. R. Corderman and J. L. Beauchamp, J. Amer. Chem. Soc. 98, 3998-4000 (1976).
10. R. R. Corderman and J. L. Beauchamp, J. Organomet. Chem., submitted for publication.
11. T. E. Orlowski, B. S. Freiser and J. L. Beauchamp, Chem. Phys. 16, 439-445 (1976).
12. B. S. Freiser and J. L. Beauchamp, J. Amer. Chem. Soc. 99, 3214-3225 (1977).
13. J. F. Wolf, R. H. Staley, I. Koppel, M. Taagepera, R. T. McIver, Jr., J. L. Beauchamp and R. W. Taft, J. Amer. Chem. Soc. 99, 5417-5429 (1977).
14. M. S. Foster and J. L. Beauchamp, J. Amer. Chem. Soc. 97, 4808-4814 (1975).
15. M. S. Foster and J. L. Beauchamp, J. Amer. Chem. Soc. 97, 4814-4817 (1975).
16. A. E. Stevens and J. L. Beauchamp, J. Amer. Chem. Soc., submitted for publication.
17. J. Fernando, G. Faigle, A. M. da Costa Ferreira, S. E. Galembeck and J. M. Riveros, J. Chem. Soc. Chem. Comm., 126-127 (1978).
18. J. L. Beauchamp, unpublished results.
19. A. E. Stevens and J. L. Beauchamp, unpublished results.
20. R. R. Corderman and J. L. Beauchamp, Inorg. Chem. 15, 665-668 (1976).
21. P. B. Armentrout, R. V. Hodges and J. L. Beauchamp, J. Chem. Phys. 66, 4683-4688 (1977).
22. P. B. Armentrout and J. L. Beauchamp, unpublished results.
23. J. Allison and D. P. Ridge, J. Organomet. Chem. 99, C11-C14 (1975).
24. F. A. Houle and J. L. Beauchamp, J. Amer. Chem. Soc., submitted for publication.
25. R. L. Woodin and J. L. Beauchamp, J. Amer. Chem. Soc. 100, 501-508 (1978).
26. M. Elian, M. M. L. Chen, D. M. P. Mingos and R. Hoffmann, Inorg. Chem. 15, 1148-1155 (1976).
27. A. E. Stevens and J. L. Beauchamp, unpublished results.
28. R. R. Corderman and J. L. Beauchamp, Inorg. Chem. 17, 68-70 (1978).
29. R. R. Corderman and J. L. Beauchamp, J. Amer. Chem. Soc. 98, 5700-5702 (1976).
30. R. W. Johnson and R. G. Pearson, Inorg. Chem. 10, 2091-2095 (1971).
31. A. Davison, W. McFarlane, L. Pratt and G. Wilkinson, J. Chem. Soc. 3653-3666 (1962).
32. J. L. Beauchamp, D. Holtz, S. D. Woodgate and S. L. Patt, J. Amer. Chem. Soc. 94, 2798-2807 (1972).